Distal transport of dissolved hydrothermal iron in the deep South Pacific Ocean

Jessica N. Fitzsimmons[a,b,1], Edward A. Boyle[b,1], and William J. Jenkins[c]

[a]Institute of Marine and Coastal Sciences, Rutgers University, New Brunswick, NJ 08901; [b]Department of Earth, Atmospheric, and Planetary Sciences, Massachusetts Institute of Technology, Cambridge, MA 02139; and [c]Marine Chemistry and Geochemistry, Woods Hole Oceanographic Institution, Woods Hole, MA 02543

This contribution is part of the special series of Inaugural Articles by members of the National Academy of Sciences elected in 2008.

Contributed by Edward A. Boyle, September 30, 2014 (sent for review April 17, 2014; reviewed by Brandy M. Toner and John Lupton)

Until recently, hydrothermal vents were not considered to be an important source to the marine dissolved Fe (dFe) inventory because hydrothermal Fe was believed to precipitate quantitatively near the vent site. Based on recent abyssal dFe enrichments near hydrothermal vents, however, the leaky vent hypothesis [Toner BM, et al. (2012) *Oceanography* 25(1):209–212] argues that some hydrothermal Fe persists in the dissolved phase and contributes a significant flux of dFe to the global ocean. We show here the first, to our knowledge, dFe (<0.4 μm) measurements from the abyssal southeast and southwest Pacific Ocean, where dFe of 1.0–1.5 nmol/kg near 2,000 m depth (0.4–0.9 nmol/kg above typical deep-sea dFe concentrations) was determined to be hydrothermally derived based on its correlation with primordial ^{3}He and dissolved Mn (dFe:^{3}He of 0.9–2.7 × 10^6). Given the known sites of hydrothermal venting in these regions, this dFe must have been transported thousands of kilometers away from its vent site to reach our sampling stations. Additionally, changes in the size partitioning of the hydrothermal dFe between soluble (<0.02 μm) and colloidal (0.02–0.4 μm) phases with increasing distance from the vents indicate that dFe transformations continue to occur far from the vent source. This study confirms that although the southern East Pacific Rise only leaks 0.02–1% of total Fe vented into the abyssal Pacific, this dFe persists thousands of kilometers away from the vent source with sufficient magnitude that hydrothermal vents can have far-field effects on global dFe distributions and inventories (≥3% of global aerosol dFe input).

iron | hydrothermal vents | helium | East Pacific Rise | trace metals

Low concentrations of the micronutrient iron in seawater are known to limit primary production and nitrogen fixation in large regions of the global ocean (1, 2). As a result, the marine dissolved Fe (dFe) distribution indirectly influences global climate because it serves to modulate the metabolic success of phytoplankton that sequester carbon into the deep ocean, both in the modern era and during the geologic past (3). The marine dFe distribution is controlled by a balance of Fe sinks, namely, biological uptake, scavenging, and precipitation to the particulate phase, and Fe sources, largely arising from atmospheric dust deposition over the ocean and continental margin Fe fluxes (4).

Black smoker hydrothermal vents exude fluids with μM–mM Fe concentrations (5, 6), which can be as much as seven orders of magnitude greater in Fe concentration than typical deep ocean dFe of ∼0.2–0.8 nM (7–10). Thus, only a small fraction of hydrothermal Fe would need to escape precipitation to significantly alter oceanic dFe distributions. For decades, however, hydrothermal Fe has been neglected as a major source of dFe to the open ocean because it was thought to precipitate quantitatively as particulate sulfides or oxides near the vent site upon mixing with seawater (11, 12), leaving no residual trace in the dissolved phase.

However, in recent years with the advent of high-resolution sampling and analysis of trace metals, abyssal hot spots of enhanced dFe concentration >1 nmol/kg have been detected near known vent sites in the Pacific (13–15), Atlantic (8, 16), Indian (17), Arctic (18), and Southern Oceans (10), clearly demonstrating that hydrothermal venting increases deep-sea dFe concentrations proximal to vent sites. This led to the development of the leaky vent hypothesis (19), which posits that some hydrothermal Fe may persist in the dissolved phase that contributes significantly to the deep ocean dFe inventory. Hydrothermal inputs to the dFe phase have even been modeled along fast-spreading (20) and slow-spreading (16) ridges. Assuming that these models' parameterization of dFe scavenging is valid for hydrothermal dFe, this vent-derived dFe should persist thousands of kilometers from the vent source, even reaching the biologically active euphotic zone where dFe is a required micronutrient. This potentially significant effect of hydrothermal dFe on global Fe distributions would require that hydrothermal vents be considered an important source of dFe to the global ocean. However, no abyssal dFe measurements have sufficiently demonstrated that hydrothermal dFe does persist thousands of kilometers from its vent site to prove the leaky vent hypothesis or ground truth these models. This shortcoming results from both a weak understanding of the global distribution of hydrothermal vents and a dearth of trace metal sampling along distal hydrothermal plumes in the deep ocean.

Following the earlier description by Boyle and Jenkins (15), we address this problem by reporting the deep ocean dFe concentrations in the South Pacific Ocean, where no measurements of dFe concentration deeper than 1,000 m have been reported previously (21). In the South Pacific, the East Pacific Rise (EPR) supports extensive hydrothermal activity, and distal transport of

Significance

Low concentrations of the micronutrient iron in seawater are known to limit primary production and nitrogen fixation in large regions of the global ocean. Thus, it is important to constrain the sources and sinks controlling the marine dissolved iron distribution and consequent micronutrient supply to surface plankton. Although the major dissolved iron sources have been historically thought to be atmospheric dust inputs and fluxes from the continental margin, we show here the first data to our knowledge demonstrating that dissolved iron from hydrothermal vents can be transported thousands of kilometers from the venting site, which to date has only been suggested and modeled. Thus, hydrothermal vents must be considered when determining the marine dissolved iron inventory, especially in the abyssal ocean.

Author contributions: J.N.F., E.A.B., and W.J.J. designed research, performed research, analyzed data, and wrote the paper.

Reviewers: B.M.T., University of Minnesota; and J.L., National Oceanic and Atmospheric Administration Pacific Marine Environmental Laboratory.

The authors declare no conflict of interest.

See Commentary on page 16641.

[1]To whom correspondence may be addressed. Email: eaboyle@mit.edu or jessfitz@mit.edu.

This article contains supporting information online at www.pnas.org/lookup/suppl/doi:10.1073/pnas.1418778111/-/DCSupplemental.

hydrothermal dFe might be especially promoted there because Fe(II) lifetimes are near their longest in the open ocean due to low oxygen concentrations following microbial consumption along global overturning circulation (22). Moreover, the South Pacific Ocean is an important place to determine the influence of hydrothermal Fe injection on ocean productivity and climate because abyssal Southern Hemisphere water masses eventually upwell into the Fe-limited Southern Ocean. Thus, South Pacific dFe enrichments from hydrothermal venting have the potential to fuel increased productivity and carbon export in the Fe-limited Southern Ocean (20), where an understanding of the processes stimulating primary production is still an active area of research, both on modern and geologic timescales (3, 23–25).

Results and Discussion

Enhanced dFe concentrations (filtered with a pore size of 0.4 μm) of 1.0–1.5 nmol/kg were found centered at ∼2,000 m depth at three stations in the South Pacific: KM0703 SPEEDO Station 19 (20°S, 170°W) in the western South Pacific and Melville BiG RAPA Stations 4 (23.5°S, 88.75°W) and 7 (26.25°S, 104°W) in the eastern South Pacific (station map in Fig. 1; Fe data in Fig. 2). These dFe concentrations are elevated above typical North Pacific (7, 13) and Atlantic (8, 9, 26) abyssal dFe concentrations of 0.3–0.6 nmol/kg and thus connote a clear dFe anomaly.

The 2,000-m dFe maxima at these sites are not coincident with apparent oxygen utilization (AOU) maxima at 500–1,000 m and thus cannot be caused by the remineralization of Fe from sinking organic material (Fig. 2). In fact, at all stations the "ferricline" (the relatively abrupt increase in dFe with depth) occurs at 400–500 m depth, corresponding exactly with the depths of rapidly increasing AOU and phosphate concentrations, such that dFe, AOU, and phosphate all reach relative maxima by 1,000 m. This 500–1,000 m ferricline also matches ferricline depths recorded in prior studies of the southeast (27) and equatorial Pacific (14) and is attributed to remineralization of sinking organic matter. Like phosphate and AOU, remineralization-derived dFe concentrations stabilize between 500 and 1,000 m at concentrations of 0.3 nmol/kg at Stations 7 and 19 and 0.6 nmol/kg at Station 4. As expected in a remineralization-dominated region, dFe and AOU have a linear relationship along these depths (Fig. 3, solid circles) that results in calculated seawater dFe:C ratios of 2.4–4.5 × 10^{-6}, falling within the 1.4–4.7 × 10^{-6} range observed in the North and equatorial Pacific (28).

Below these remineralization-dominated depths, dFe increases again to anomalously enriched values of ∼1.0–1.5 nmol/kg at 2,000 m, most of which we suggest is contributed by the distal transport of hydrothermally vented Fe from the East Pacific Rise (EPR). We base this hypothesis on several lines of evidence. First, the enriched dFe data near 2,000 m (shown as crosses in Fig. 3) fall off the linear relationship of dFe:AOU, indicating that the high Fe concentrations are not produced by remineralization. If these dFe data are included in the Fe:C ratio estimates, not only do the linear correlations between dFe and AOU have much greater errors, but the resulting Fe:C ratios (designated as "Fe:C (all)" in Fig. 3) also increase to 5.1–9.2 × 10^{-6}, which is higher than has ever been recorded in the open ocean Pacific (28).

Additionally, the dFe profiles show striking similarities to profiles of excess ^{3}He (Figs. 4*A* and 2), which is derived from primordial degassing at hydrothermally active sites (29). The ^{3}He data were not measured from the same samples as dFe but were taken from archive Pacific Ocean datasets and interpolated quantitatively onto the locations and depths of dFe measurement (*Methods* and Fig. 1); we assume that the abyssal ^{3}He distributions are smooth and stable over the timescales of these measurements. The coincident ^{3}He and dFe maxima at 2,000 m point to a hydrothermal dFe source. A concomitant enrichment in dissolved manganese (dMn) at 2,000 m depth (Fig. 2) further corroborates the hypothesis of hydrothermal influence because Mn is also released from vents at high concentrations (5, 30) but otherwise has low deep ocean concentrations (31) (Mn data and Fe/Mn ratios are discussed further in *SI Text*). These correlated dFe, dMn, and ^{3}He profiles (Fig. 2) confirm that hydrothermal venting enriches dFe by 0.4–0.9 nmol/kg above background concentrations in the abyssal South Pacific Ocean, which is even larger than the 0.1–0.5 nmol/kg enrichments estimated by the

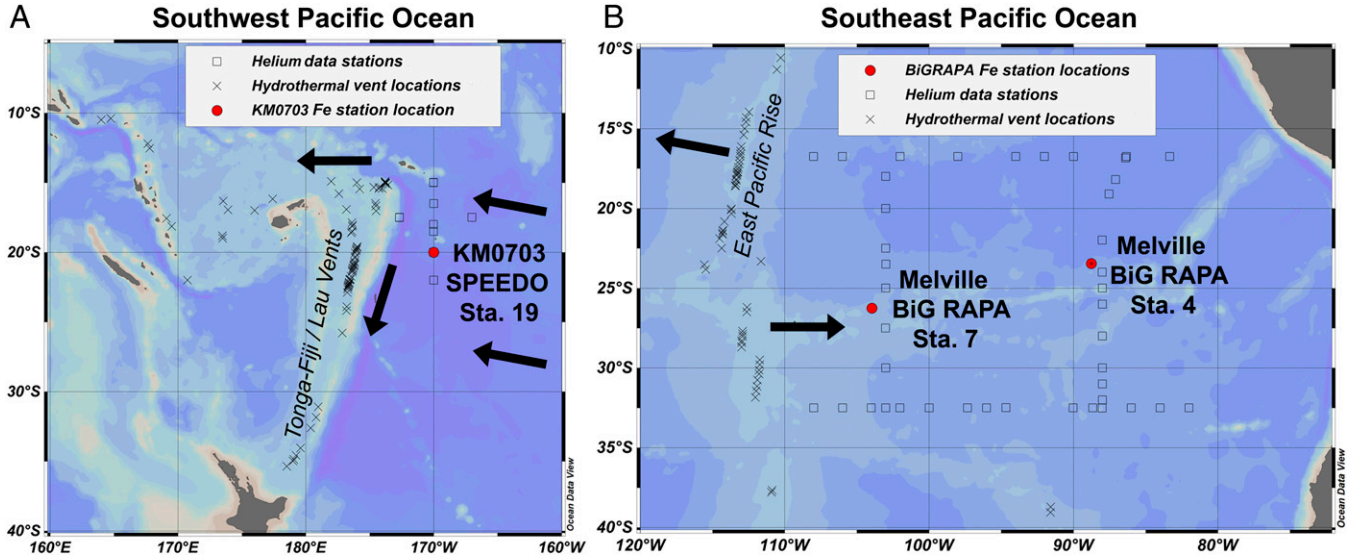

Fig. 1. Map of study locations. (*A*) The southwest Pacific, where KM0703 SPEEDO Station 19 (20°S, 170°W) is indicated in red and the hydrothermally active Tonga–Kermadec Arc is indicated as a topographic high along 175°W. (*B*) The southeast Pacific, where Melville BiG RAPA Stations 7 (26.25°S, 104°W) and 4 (23.5°S, 88.75°W) are indicated in red and the hydrothermally active EPR is designated. Shown as squares are stations of historical ^{3}He data that were used to interpolate the average ^{3}He profiles onto this study's sampling locations (historic ^{3}He data from cchdo.ucsd.edu); the more proximal stations had a greater influence on the interpolated ^{3}He profile than the distal stations. Shown as crosses are sites of confirmed or inferred hydrothermal venting deeper than 1,000 m (33). Directions of mean advection at 2,000 m (36) are indicated with black arrows.

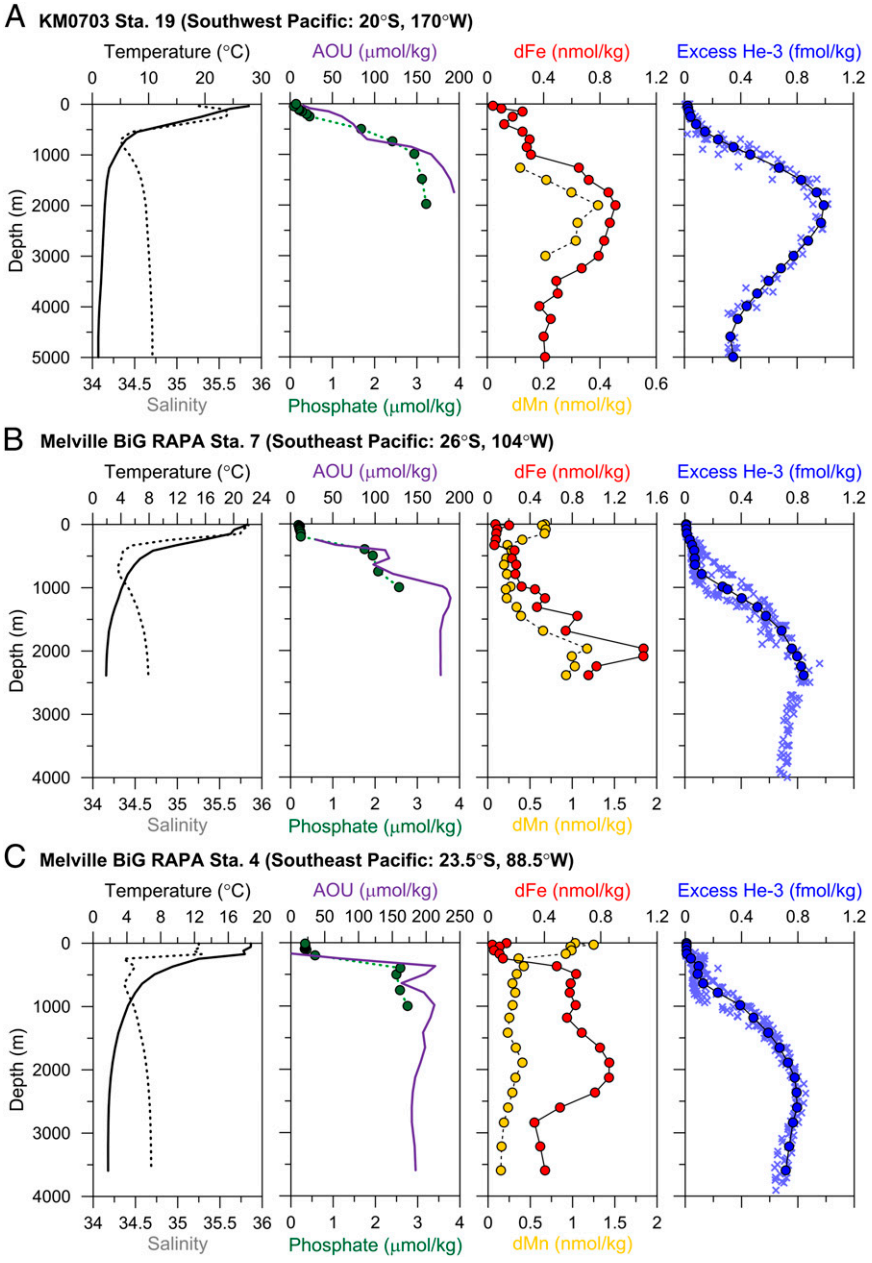

Fig. 2. Oceanographic profiles showing a hydrothermal influence on dFe, ^{3}He, and dMn at 2,000 m. Relevant profiles taken from (*A*) SPEEDO-KM0703 Station 19 in the southwest Pacific, (*B*) Melville BiG RAPA Station 7 in the southeast Pacific, and (*C*) Melville BiG RAPA Station 4 in the southeast Pacific. Note that dFe SDs on replicate analyses (tabulated in Table S1) were typically the size of the symbol and are thus not shown. The interpolated excess ^{3}He data are shown as blue circles at the depths where dFe measurements were made, whereas the data used to generate those average values are shown as light blue crosses.

recent model of hydrothermal Fe delivery to the deep ocean from fast-spreading ridges (20).

Elevated dFe concentrations near sites of hydrothermal venting have previously been observed in the abyssal Pacific (13, 14, 32). What makes the South Pacific dFe data of this study truly remarkable, however, is that they are sampled from locations hundreds to thousands of kilometers from the nearest known vent source, and they still demonstrate elevated dFe concentrations of ∼1.0–1.5 nmol/kg. Although we cannot prove exactly which vents contributed to the observed distal dFe maxima, we hypothesize below and in *SI Text* which vent regions most likely sourced the dFe based on knowledge of the abyssal circulation (33), and we show that the dFe must have traveled extreme distances to reach the sampling locations, supporting the leaky vent hypothesis. Transit times (t) from the vent sites are also estimated, assuming a conservatively slow off-axis abyssal South Pacific current speed of 2 mm/s (34) (thus, calculated transit times are maximum times). This allows an assessment of whether dFe would be expected to have survived scavenging, given typical abyssal dFe residence times of 70–270 y (7, 35).

KM0703 SPEEDO Station 19 in the western South Pacific receives the majority of its hydrothermal influence from southern EPR hydrothermal vents (∼15°S) that travel more than 6,000 km from the east (t > 95 y) at 2,000–3,500 m depth. Despite being only 600–700 km to the east of Lau Basin vent sources, abyssal circulation moves hydrothermal plumes from the Lau Basin westward and away from KM0703 Station 19, as determined by both steric height calculations (36) and ^{3}He data

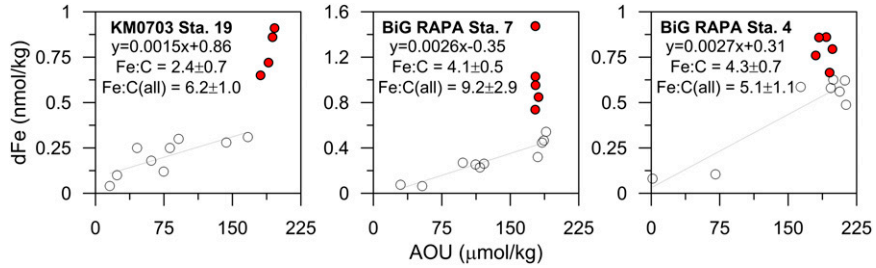

Fig. 3. dFe–AOU relationships for each of the three sampling locations: (*Left*) SPEEDO-KM0703 Station 19 in the southwest Pacific, (*Middle*) Melville BiG RAPA Station 7 in the southeast Pacific, and (*Right*) Melville BiG RAPA Station 4 in the southeast Pacific. The stations included in the Fe:C regression calculation are in open circles (~500–1,000 m depth), whereas the red circles show the deeper sample depths affected by hydrothermal Fe; these correspond to the equivalent symbols in Fig. 4. The Fe:C ratio is derived from the regression (open circles only), whereas the ratio indicated as "Fe:C (all)" includes all points (even those experiencing hydrothermal Fe inputs in red). Fe:C ratios are calculated using an AOU:C ratio of 1.6 (61) and are in units of μmol/mol.

(37). The ultimate sources of KM0703 Station 19 dFe and ^{3}He maxima, then, must be the hydrothermal activity occurring near 15°S (38), which forms a well-established hydrothermal plume across the Pacific.

Melville BiG RAPA Stations 4 and 7 in the southeast Pacific also have a clear southern EPR source. Despite the westward trajectory of southern EPR hydrothermal plumes near ~15°S (38), circulation studies using steric height estimations (39) have determined that south of 20°S, enhanced abyssal ^{3}He as well as enriched Fe/Mn oxides in sediments to the east of the EPR in the Peru/Chile Basins are derived from eastward advection of EPR plumes (29). Thus, an eastward flowing EPR Fe source near 25°S would have to travel at least 800 km to influence Station 7 (t = 12.5 y) and over 2,400 km to influence Station 4 (t = 38 y), although we cannot confirm that hydrothermal dFe values at Stations 4 and 7 are derived from the same vent site. Thus, in the South Pacific, not only is hydrothermal Fe maintained in the dissolved phase locally at the vent site, but it is able to escape scavenging and be transported hundreds to several thousands of kilometers from the vent site, all while maintaining elevated dFe concentrations.

How is this Fe stabilization in the dissolved phase achieved? Two hypotheses have been proposed, and likely both contribute to hydrothermal dFe stabilization. First, pyrite nanoparticles between 4 and 200 nm have been shown to account for 5–25% of

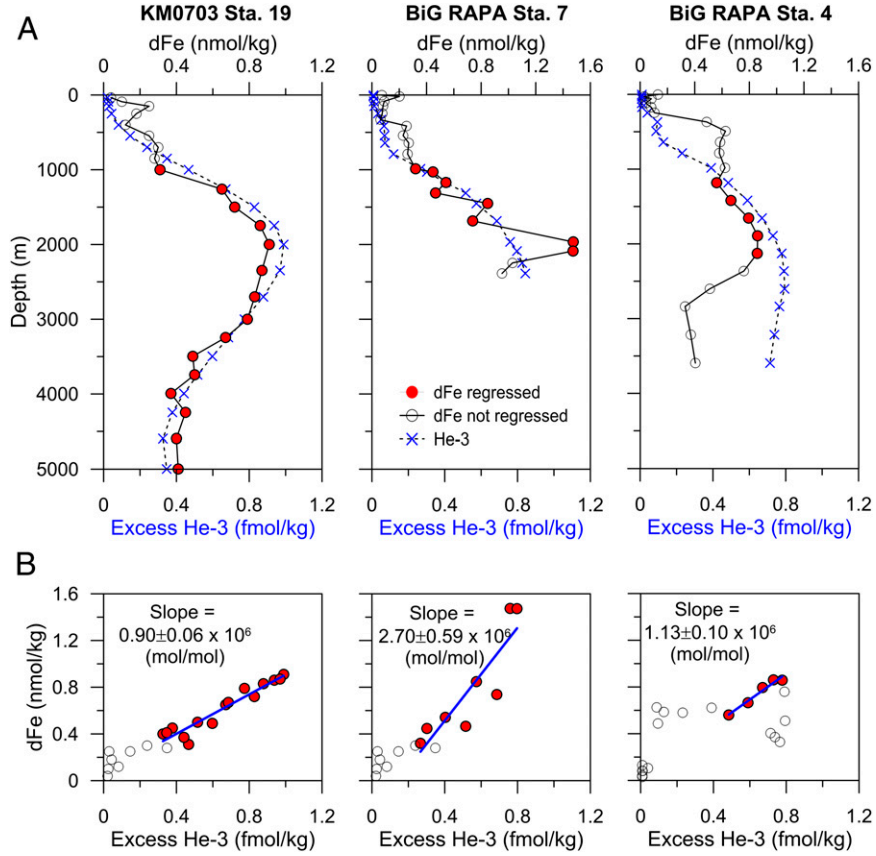

Fig. 4. Distal hydrothermal dFe/^{3}He. (*A*) dFe and ^{3}He data and (*B*) the Type II regressions used to evolve dFe/^{3}He ratios. Station locations are (*Left*) KM0703 Station 19 in the southwest Pacific, (*Middle*) BiG RAPA Station 7 in the southeast Pacific, and (*Right*) BiG RAPA Station 4 in the southeast Pacific. Data excluded from the dFe/^{3}He regression calculation are shown in both *A* and *B* as open circles and include all data shallower than 1,000 m and the deepest samples of Stations 4 and 7, where dFe appears to have been scavenged, while ^{3}He remains elevated.

the dFe in global vent fluids (40, 41). These colloids would pass through the 0.4-μm filter used to operationally define dissolved Fe in this study, and due to their small size they would sink very slowly, providing a mechanism by which inorganic dFe might be carried away from vents in the dissolved fraction. Potentially a more ubiquitous pathway, recent studies have shown that organic ligands bind 4–8% of the dissolved Fe in hydrothermal plumes (42–44). This organic chelation protects the Fe from precipitation and stabilizes it in the dissolved phase as it is advected away from the vent site. Particulate Fe(II) (>0.4 μm) has also been shown to be protected from oxidation by organic compounds near hydrothermal vents (45), further emphasizing the role of organics in stabilizing hydrothermal Fe species. A recent study has even implicated the microbial iron pump near deep-sea hydrothermal vents in converting hydrothermal Fe into dissolved Fe–C complexes (46).

To further investigate the mechanism of hydrothermal dissolved Fe stabilization, we measured the size partitioning of dFe between soluble Fe (sFe, <0.02 μm) and colloidal Fe phases (0.02 μm < cFe < 0.4 μm; cFe = dFe − sFe). sFe is typically considered to be truly dissolved, whereas cFe is composed of particles so small that they remain suspended in solution and are circulated and collected along with the dissolved Fe pool; both inorganic and organically bound dFe can be present in both size fractions. The size partitioning results shown in Fig. 5 suggest that when hydrothermally derived dFe is high (Station 7), colloidal Fe is the dominant dFe fraction (cFe composes 76% of dFe), whereas a more diluted/scavenged dFe signal (Stations 19 and 4) has a more soluble Fe-rich dFe pool (50% soluble, 50% colloidal Fe). Thus, assuming a similarly partitioned Fe source among the three stations studied here, colloidal Fe appears to compose most of the dFe near the vent site (Station 7) and is transformed into a soluble Fe maximum (Station 4) as the dFe is scavenged away farther from the vents. These observations are consistent with the two published near-field Fe size partitioning studies, both of which demonstrated that near the site of hydrothermal venting colloidal Fe is the primary dFe phase (42, 47).

In the southeast Pacific, not only does percentage soluble Fe (sFe/dFe) increase with distance from the vents, but the absolute sFe concentration also increases with distance from the vent, rising from 0.35 nmol/kg at Melville BiG RAPA Station 7 to a sFe maximum of 0.51 nmol/kg at Station 4. This Station 4 sFe concentration and the 0.44 nmol/kg sFe at Station 19 are well above background abyssal sFe concentrations in the Pacific of 0.2–0.3 nmol/kg (48) and must have been transferred from the particulate (pFe) or colloidal fraction. This downstream sFe amplification leads us to conclude that interphase Fe transformations not only occur at the local site of hydrothermal venting but must continue hundreds to thousands of kilometers from the vent source. The nature of these pFe, sFe, and cFe transformations are unknown, but potential mechanisms that could explain the observed pattern include the chelation of Fe in inorganic colloids by truly soluble organic compounds over time/distance and/or the exchange between soluble and colloidal organically bound Fe complexes. These data support the recent theory that exchange processes between sFe and cFe commonly transform marine dFe toward a 50–50% sFe–cFe partitioning, provided sufficient time and an absence of external dFe sources (49, 50).

To evaluate the extent of scavenging of dFe along these trajectories, we compared our dFe distributions to excess ^{3}He concentration, which is a conservative tracer of hydrothermal input to the abyssal ocean. Excess ^{3}He values measured from nearby World Ocean Circulation Experiment stations were interpolated onto the depths and locations of the measured dFe data (see Fig. 1 for the locations of ^{3}He profiles and Fig. 2 for the ^{3}He interpolation), and dFe/^{3}He ratios were determined (Fig. 4*B*). Only depths near the hydrothermally derived dFe maxima (Fig. 4, filled circles) were included in the regression calculation to avoid the influence of upper ocean biological processing and subplume Fe scavenging on the observed dFe. Resulting dFe/^{3}He ratios ranged from a Fe/^{3}He molar ratio of 0.9–2.7 × 10^{6}, which are much lower than the 2–10 × 10^{8} values found in high-temperature vent fluids (both at EPR 19°S and in the western Pacific vents (20)). Thus,

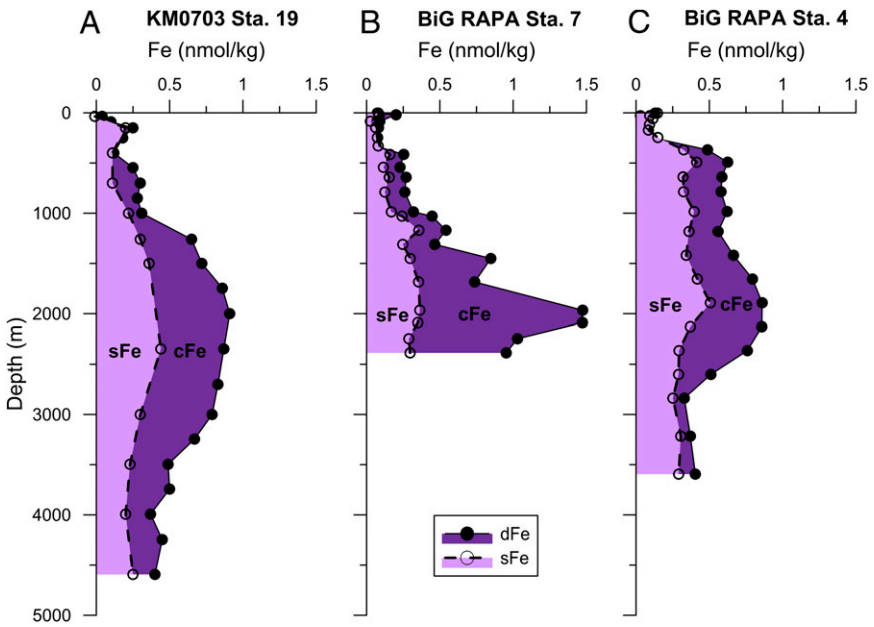

Fig. 5. The size partitioning of dFe into soluble and colloidal phases demonstrates continued Fe transformations at great distance from vents. Dissolved Fe (closed circles, solid line; dFe < 0.4 μm) is partitioned into soluble Fe (open circles, dashed line, light purple shading; sFe < 0.02 μm or 10 kDa) and colloidal Fe (cFe, the difference between the two lines in dark purple shading) fractions at (*A*) Station 19 in the southwest Pacific, (*B*) Station 7 in the southeast Pacific, and (*C*) Station 4 in the southeast Pacific. SDs are typically the size of the symbol and are thus not shown.

only 0.02–1.0% of total vented hydrothermal Fe survives transport hundreds to thousands of kilometers away in the dissolved phase. Even within the three far-field stations of this study, the dFe/^{3}He ratios decrease with increasing distance from the vent source, with the lowest ratio representing a distally persistent, scavenging-influenced hydrothermal signal.

It is worth noting that in the southwest Pacific the ^{3}He and dFe profiles are nearly identical, whereas in the southeast Pacific the ^{3}He remains elevated to the bottom, while dFe decreases to background concentrations below 2,500–3,000 m. An elevated ^{3}He signal in the absence of Fe enrichment implies dFe scavenging. The depth range of this dFe–^{3}He decoupling (3,000–4000 m; Fig. 4*A*) is below the typical sill depth of the southern EPR and Chile Ridge (2,500–3,000 m), and thus we hypothesize that the ^{3}He measured below those depths may be relic ^{3}He that reached those depths after long circulation times during which the He was mixed conservatively but the hydrothermal dFe was scavenged [deep ocean residence time of dFe is 70–270 y (7, 35)].

The results of this study support a leaky vent model of dFe inputs to the abyssal South Pacific Ocean and also demonstrate transport of hydrothermal Fe in the dissolved phase up to 6,000 km from the vent source. If the dFe/^{3}He ratio of 0.9×10^6 mol/mol is indicative of the amount of vent-derived dFe persisting along hydrothermal plumes, then using the estimated annual loss rate of ^{3}He from the ocean (51) of 750 ± 200 mol/y, we estimate that the flux of dFe leaking from global vents into the deep ocean is $\sim 7 \times 10^8$ mol/y. This value is twice the hydrothermal flux reported based on Fe-binding ligand measurements near the Mid-Atlantic Ridge (43) and is ∼3% of the estimated 2.36×10^{10} mol/y aerosol inputs of dissolved Fe into the surface ocean (21). Although this might seem to be a relatively insignificant marine Fe source compared with dust, we know that abyssal Southern Hemisphere waters eventually upwell in the Fe-limited Southern Ocean (20) where upper ocean productivity plays a significant role in global carbon export (52), allowing the relatively small percentage of open ocean dFe contributed by hydrothermal vents calculated here to play a disproportionately large role in global climate by its influence in the Fe-limited Southern Ocean. If this persistent hydrothermal dFe were to reach the surface and fertilize phytoplankton with an Fe:C ratio of 6 μmol Fe per mol carbon [typical of blooming diatoms in the Fe-limited Southern Ocean (53)], this dFe could support $\sim 1 \times 10^{14}$ mol/y of new carbon, which is comparable in magnitude to global new production (4×10^{14} mol/y) (54).

This estimate of $\sim 7 \times 10^8$ mol/y leaky dFe flux from hydrothermal vents, however, has both positive and negative uncertainties. dFe/^{3}He ratios vary globally as a function of bedrock geology and ridge spreading rate, and values along the slow-spreading Mid-Atlantic Ridge (16) have been found to be as much as 78× higher than those in the Pacific, indicating that the global estimate of hydrothermal Fe inputs to the dFe inventory calculated here is biased low. Assuming our lowest Fe/^{3}He ratio of 0.9×10^6 and an Atlantic ratio of 70×10^6 mol/mol, Saito et al. (16) calculated a slightly higher hydrothermal dFe flux of 9×10^8 mol/y. In contrast, our carbon new production estimate may be biased high since it assumes full biological availability of the hydrothermal dFe, which might not be true if the dFe was in an inorganic nanoparticulate form (55). However, potentially the largest problem with these flux estimates is the poor constraint of scavenging rates of hydrothermal dFe, which depend on both Fe speciation and deep water biogeochemical conditions. We have little information about which chemical features control the persistence of hydrothermal dFe, and we know even less about the relative rates of scavenging for hydrothermal dFe compared with typical abyssal dFe, so it is difficult to determine which dFe/^{3}He ratios are most applicable to these flux calculations. Common abyssal dFe is scavenged onto sinking particles over 70–270 y (7, 35), so scavenging of some portion of this persistent hydrothermal dFe is likely before upwelling to the surface ocean. Only more studies of dFe/^{3}He distributions in the abyssal ocean can reveal whether a persistent ratio is ever reached upon plume dilution as well as the global distributions of this ratio.

In this study we showed that hydrothermally derived dFe is transported thousands of kilometers from the vent source in the South Pacific Ocean, in support of the leaky vent hypothesis as well as recent models implying a significant hydrothermal Fe source to the oceanic dFe budget. The mechanism of dFe stabilization is an active area of investigation, and size partitioning dFe data from this study further indicate that Fe transformations continue to occur at great distance from the vent source (namely, transformations of colloidal or particulate Fe near the vent site to soluble Fe distally). Future research must focus on distal hydrothermal dFe transformation pathways and especially scavenging rates to constrain the spatial and temporal extent of this abyssal dFe source. Additionally, global Fe and climate models that have neglected hydrothermal Fe inputs require its future inclusion.

Methods

The stations discussed in this paper were collected on two cruises sponsored by the Center for Microbial Oceanography: Research and Education (C-MORE) and were the only abyssal open ocean stations sampled on these cruises. Station 19 in the southwest Pacific was sampled on the R/V *Kilo Moana* in April 2007 on the C-MORE SPEEDO cruise, and Stations 4 and 7 in the southeast Pacific were sampled on the R/V *Melville* in November–December 2010 on the C-MORE BiG RAPA cruise. Trace metal-uncontaminated seawater was collected on KM0703 using the Moored in situ trace element serial sampler (MITESS) system (56) and filtered through 0.4-μm Nuclepore filters into Teflon or high-density polyethylene (HDPE) bottles by previously established methods (57) (Teflon vs. HDPE bottles indicated in Table S1). Soluble Fe samples were collected after filtration through a 0.02-μm Anodisc filter. On the Melville BiG RAPA cruise, seawater was collected using the MITESS/Vanes system and filtered through 0.4-μm Nuclepore filters into HDPE bottles (57). Soluble Fe samples were collected using a cross-flow ultrafiltration system in static mode using a 10-kDa nominal molecular weight cutoff regenerated cellulose filter (Pellicon XL, PLCGC; Millipore) after conditioning with 350 mL of filtered sample seawater. Detailed methodological descriptions and an intercalibration between the two soluble Fe sample collection methods used in this study have been described previously (58).

Samples were analyzed in triplicate for their Fe concentration by isotope dilution inductively coupled plasma mass spectrometry (ID-ICP-MS) on a hexapole collision cell IsoProbe ICP-MS. The ID-ICP-MS method employs an ^{54}Fe spike and batch preconcentration with nitrilotriacetate resin (59). Procedure blanks for the western Pacific stations were 0.20 nmol/kg but very stable to ±0.03 nmol/kg because they derived quantitatively from the constant amount of NTA Superflow resin used to preconcentrate the Fe. Procedure blanks over the six analytical sessions for the eastern Pacific stations were much lower, ranging from 0.025 to 0.060 nmol/kg, and the detection limit (three times the SD of the procedure blanks for each analytical session) averaged 0.025 nmol/kg. Comprehensive laboratory analyses of SAFe D2 standard for dFe during the period of these analyses averaged 0.99 ± 0.03 nmol/kg (Bottle 242, ±1 SD, $n = 8$) and 0.92 ± 0.01 nmol/kg (Bottle 446, ±1 SD, $n = 8$), which agrees well with the current consensus value of 0.933 ± 0.023 nmol/kg (May 2013 consensus: www.geotraces.org/science/intercalibration).

Dissolved manganese (dMn) was extracted from filtered seawater by a modified version of an automated flow injection preconcentration method (60), followed by dMn concentration analysis using quadrupole ICP-MS and standard addition calibrations. The 12 mL filtered and acidified samples were pipetted into acid-cleaned 50-mL Corning centrifuge tubes. To generate standard curves throughout the run, 60, 120, and 180 μL of 100 nM Mn standard were added to SAFe surface water; this allowed for final Mn standard concentrations of 0.5, 1.0, and 1.5 nM, respectively. The pH of each sample was brought to 6.0 ± 0.2 with ammonium acetate buffer (pH 8.9) before being pumped through the extraction system. The extraction system was identical to that described by Milne et al. (60), except that the microcolumn was filled with Nobias-chelate PA1 resin (Elemental Scientific). After elution through the column in 1.0 mL of 1M 4×-distilled nitric acid, extracted samples were analyzed for dMn by ICP-MS on a VG/Fisons PQ2+. The SAFe D1 standard reference seawater was found to have a dMn concentration of 0.352 ± 0.020 nmol/kg ($n = 8$; ±1 SD of replicate analyses), agreeing

exactly with the SAFe D2 consensus value of 0.35 ± 0.05 nmol/kg. dMn procedure blanks were less than 0.01 nmol/kg.

The ^{3}He data were obtained from cchdo.ucsd.edu/ (see also the measurement protocols described at cchdo.ucsd.edu/manuals/pdf/91_1/jenknew.pdf), and the stations in the vicinity of the dFe stations (Fig. 1) were used to interpolate onto the dFe station data in the following manner. First, excess ^{3}He was computed using the reported the helium isotope ratio anomaly and helium concentration, correcting for helium solubility isotope fractionation at equilibrium with air, and then each ^{3}He station was vertically interpolated onto neutral density surfaces. Next, the distribution of excess ^{3}He on each isopycnal surface was interpolated to the geographic location of the dFe stations; although all ^{3}He stations (squares) in Fig. 1 were used in the interpolation, the more proximal stations had a greater influence on the resulting ^{3}He profile than the distal stations. Finally, the resultant profiles of ^{3}He vs. neutral density were interpolated to the sampling depths of the dFe profiles. The statistical uncertainties associated with this interpolation were small relative to the variance in the dFe:^{3}He relationships subsequently derived.

ACKNOWLEDGMENTS. We thank Jong-Mi Lee and Rick Kayser for collecting and filtering samples on the BiG RAPA cruise, Dan Repeta, who served as chief scientist on the Melville BiG RAPA cruise, and Jon Zehr and Joe Montoya, who served as chief scientists on the KM0703 SPEEDO cruise. We also thank Chris German for comments on an early draft of this manuscript. Finally, we thank the officers and crew of the R/V *Kilo Moana* and the R/V *Melville* for their efforts on our behalf. This work was funded by a National Science Foundation (NSF) Graduate Research Fellowship (NSF Award 0645960) and the Center for Microbial Oceanography: Research and Education (NSF-OIA Award EF-0424599). E.A.B.'s participation in the SPEEDO cruise was funded by a Gordon and Betty Moore Foundation grant to Jon Zehr.

1. Moore JK, Doney SC, Glover DM, Fung IY (2002) Iron cycling and nutrient-limitation patterns in surface waters of the World Ocean. *Deep Sea Res Part II Top Stud Oceanogr* 49(1-3):463–507.
2. Boyd PW, et al. (2007) Mesoscale iron enrichment experiments 1993-2005: Synthesis and future directions. *Science* 315(5812):612–617.
3. Martin JH (1990) Glacial-interglacial CO_2 change: The iron hypothesis. *Paleoceanography* 5(1):1–13.
4. Moore JK, Doney SC, Lindsay K (2004) Upper ocean ecosystem dynamics and iron cycling in a global three-dimensional model. *Global Biogeochem Cycles* 18(4): GB4028.
5. Von Damm KL, et al. (1985) Chemistry of submarine hydrothermal solutions at 21°N, East Pacific Rise. *Geochim Cosmochim Acta* 49(11):2197–2220.
6. Douville E, et al. (2002) The rainbow vent fluids (36°14′N, MAR): The influence of ultramafic rocks and phase separation on trace metal content in Mid-Atlantic Ridge hydrothermal fluids. *Chem Geol* 184(1-2):37–48.
7. Bruland KW, Orians KJ, Cowen JP (1994) Reactive trace metals in the stratified central North Pacific. *Geochim Cosmochim Acta* 58(15):3171–3182.
8. Hatta M, et al. An overview of dissolved Fe and Mn distributions during the 2010-2011 U.S. GEOTRACES North Atlantic cruises. *Deep Sea Res II*, in press.
9. Noble AE, et al. (2012) Basin-scale inputs of cobalt, iron, and manganese from the Benguela-Angola front to the South Atlantic Ocean. *Limnol Oceanogr* 57(4): 989–1010.
10. Klunder MB, Laan P, Middag R, De Baar HJW, van Ooijen JC (2011) Dissolved iron in the Southern Ocean (Atlantic sector). *Deep Sea Res Part II Top Stud Oceanogr* 58(25-26):2678–2694.
11. German CR, Campbell AC, Edmond JM (1991) Hydrothermal scavenging at the Mid-Atlantic Ridge: Modification of trace element dissolved fluxes. *Earth Planet Sci Lett* 107(1):101–114.
12. Rudnicki MD, Elderfield H (1993) A chemical model of the buoyant and neutrally buoyant plume above the TAG vent field, 26 degrees N, Mid-Atlantic Ridge. *Geochim Cosmochim Acta* 57(13):2939–2957.
13. Boyle EA, Bergquist BA, Kayser RA, Mahowald N (2005) Iron, manganese, and lead at Hawaii Ocean Time-series station ALOHA: Temporal variability and an intermediate water hydrothermal plume. *Geochim Cosmochim Acta* 69(4):933–952.
14. Wu J, Wells ML, Rember R (2011) Dissolved iron anomaly in the deep tropical-subtropical Pacific: Evidence for long-range transport of hydrothermal iron. *Geochim Cosmochim Acta* 75(2):460–468.
15. Boyle EA, Jenkins WK (2008) Hydrothermal iron in the deep western South Pacific. *Geochim Cosmochim Acta* 72(12):A107.
16. Saito MA, et al. (2013) Slow-spreading submarine ridges in the South Atlantic as a significant oceanic iron source. *Nat Geosci* 6(9):775–779.
17. Nishioka J, Obata H, Tsumune D (2013) Evidence of an extensive spread of hydrothermal dissolved iron in the Indian Ocean. *Earth Planet Sci Lett* 361:26–33.
18. Klunder MB, Laan P, Middag R, de Baar HJW, Bakker K (2012) Dissolved iron in the Arctic Ocean: Important role of hydrothermal sources, shelf input and scavenging removal. *J Geophys Res* 117(C4):C04014.
19. Toner BM, Marcus MA, Edwards KJ, Rouxel O, German CR (2012) Measuring the form of iron in hydrothermal plume particles. *Oceanography* 25(1):209–212.
20. Tagliabue A, et al. (2010) Hydrothermal contribution to the oceanic dissolved iron inventory. *Nat Geosci* 3(4):252–256.
21. Moore JK, Braucher O (2008) Sedimentary and mineral dust sources of dissolved iron to the world ocean. *Biogeosciences* 5(3):631–656.
22. Field MP, Sherrell RM (2000) Dissolved and particulate Fe in a hydrothermal plume at 9°45′N, East Pacific Rise: Slow Fe (II) oxidation kinetics in Pacific plumes. *Geochim Cosmochim Acta* 64(4):619–628.
23. Boyd PW, et al. (2000) A mesoscale phytoplankton bloom in the polar Southern Ocean stimulated by iron fertilization. *Nature* 407(6805):695–702.
24. Buesseler KO, Andrews JE, Pike SM, Charette MA (2004) The effects of iron fertilization on carbon sequestration in the Southern Ocean. *Science* 304(5669):414–417.
25. Martin JH, Gordon RM, Fitzwater SE (1990) Iron in Antarctic waters. *Nature* 345(6271): 156–158.
26. Fitzsimmons JN, Zhang R, Boyle EA (2013) Dissolved iron in the tropical North Atlantic oxygen minimum zone. *Mar Chem* 154:87–99.
27. Blain S, Bonnet S, Guieu C (2008) Dissolved iron distribution in the tropical and sub tropical South Eastern Pacific. *Biogeosciences* 5(1):269–280.
28. Sunda WG (1997) Control of dissolved iron concentrations in the world ocean, A comment. *Mar Chem* 57(3-4):169–172.
29. Lupton J (1998) Hydrothermal helium plumes in the Pacific Ocean. *J Geophys Res* 103 (C8):15853–15868.
30. Edmond JM, Von Damm KL, McDuff RE, Measures CI (1982) Chemistry of hot springs on the East Pacific Rise and their effluent dispersal. *Nature* 297(5863):187–191.
31. Martin JH, Knauer GA, Broenkow WW (1985) VERTEX: The lateral transport of manganese in the northeast Pacific. *Deep Sea Res A, Oceanogr Res Pap* 32(11): 1405–1427.
32. Baker ET, et al. (2002) Hydrothermal venting along Earth's fastest spreading center: East Pacific Rise, 27.5°-32.3°S. *J Geophys Res* 107(B7):2130.
33. Beaulieu SE, Baker ET, German CR, Maffei A (2013) An authoritative global database for active submarine hydrothermal vent fields. *Geochem Geophys Geosyst* 14(11): 4892–4905.
34. Hautala SL, Riser SC (1993) A nonconservative β-spiral determination of the deep circulation in the Eastern South Pacific. *J Phys Oceanogr* 23(9):1975–2000.
35. Bergquist BA, Boyle EA (2006) Dissolved iron in the tropical and subtropical Atlantic Ocean. *Global Biogeochem Cycles* 20(1):GB1015.
36. Reid JL (1997) On the total geostrophic circulation of the Pacific Ocean: Flow patterns, tracers and transports. *Prog Oceanogr* 39(1):263–352.
37. Lupton JE, Pyle DG, Jenkins WJ, Greene R, Evans L (2004) Evidence for an extensive hydrothermal plume in the Tonga-Fiji region of the South Pacific. *Geochem Geophys Geosyst* 5(1):Q01003.
38. Lupton JE, Craig H (1981) A major helium-3 source at 15degreesS on the East Pacific Rise. *Science* 214(4516):13–18.
39. Reid JL (1986) On the total geostrophic circulation of the South Pacific Ocean: Flow patterns, tracers, and transports. *Prog Oceanogr* 16(1):1–61.
40. Gartman A, Findlay AJ, George W, Luther I (2014) Nanoparticulate pyrite and other nanoparticles are a widespread component of hydrothermal vent black smoker emissions. *Chem Geol* 366:32–41.
41. Yucel M, Gartman A, Chan CS, Luther GW (2011) Hydrothermal vents as a kinetically stable source of iron-sulphide-bearing nanoparticles to the ocean. *Nat Geosci* 4(6): 367–371.
42. Hawkes JA, Connelly DP, Gledhill M, Achterberg EP (2013) The stabilisation and transportation of dissolved iron from high temperature hydrothermal vent systems. *Earth Planet Sci Lett* 375:280–290.
43. Bennett SA, et al. (2008) The distribution and stabilisation of dissolved Fe in deep-sea hydrothermal plumes. *Earth Planet Sci Lett* 270(3-4):157–167.
44. Sander SG, Koschinsky A (2011) Metal flux from hydrothermal vents increased by organic complexation. *Nat Geosci* 4(3):145–150.
45. Toner BM, et al. (2009) Preservation of iron(II) by carbon-rich matrices in a hydrothermal plume. *Nat Geosci* 2(3):197–201.
46. Li M, et al. (2014) Microbial iron uptake as a mechanism for dispersing iron from deep-sea hydrothermal vents. *Nat Commun* 5:3192.
47. Sands CM, Connelly DP, Statham PJ, German CR (2012) Size fractionation of trace metals in the Edmond hydrothermal plume, Central Indian Ocean. *Earth Planet Sci Lett* 319-320:15–22.
48. Wu J, Boyle E, Sunda W, Wen LS (2001) Soluble and colloidal iron in the oligotrophic North Atlantic and North Pacific. *Science* 293(5531):847–849.
49. Fitzsimmons JN, Boyle EA (2014) Both soluble and colloidal iron phases control dissolved iron variability in the tropical North Atlantic Ocean. *Geochim Cosmochim Acta* 125:539–550.
50. Fitzsimmons JN, et al. Partitioning of dissolved iron and iron isotopes into soluble and colloidal phases along the GA03 GEOTRACES North Atlantic Transect. *Deep Sea Res II*, in press.
51. Craig H, Clarke WB, Beg MA (1975) Excess ^{3}He in deep water on the East Pacific Rise. *Earth Planet Sci Lett* 26(2):125–132.
52. Honjo S, Manganini SJ, Krishfield RA, Francois R (2008) Particulate organic carbon fluxes to the ocean interior and factors controlling the biological pump: A synthesis of global sediment trap programs since 1983. *Prog Oceanogr* 76(3):217–285.
53. Twining BS, Baines SB, Fisher NS (2004) Element stoichiometries of individual plankton cells collected during the southern ocean iron experiment (SOFeX). *Limnol Oceanogr* 49(6):2115–2128.
54. Shaffer G (1996) Biogeochemical cycling in the global ocean: 2. New production, Redfield ratios, and remineralization in the organic pump. *J Geophys Res* 101(C2): 3723–3745.

55. Rich HW, Morel FMM (1990) Availability of well-defined iron colloids to the marine diatom *Thalassiosira weissflogii*. *Limnol Oceanogr* 35(3):652–662.
56. Bell J, Betts J, Boyle E (2002) MITESS: A moored in situ trace element serial sampler for deep-sea moorings. *Deep Sea Res Part I Oceanogr Res Pap* 49(11):2103–2118.
57. Fitzsimmons JN, Boyle EA (2012) An intercalibration between the GEOTRACES GO-FLO and the MITESS/Vanes sampling systems for dissolved iron concentration analyses (and a closer look at adsorption effects). *Limnol Oceanogr Methods* 10: 437–450.
58. Fitzsimmons JN, Boyle EA (2014) Assessment and comparison of Anopore and cross flow filtration methods for the determination of dissolved iron size fractionation into soluble and colloidal phases in seawater. *Limnol Oceanogr Methods* 12: 244–261.
59. Lee J-M, et al. (2011) Analysis of trace metals (Cu, Cd, Pb, and Fe) in seawater using single batch nitrilotriacetate resin extraction and isotope dilution inductively coupled plasma mass spectrometry. *Anal Chim Acta* 686(1-2):93–101.
60. Milne A, Landing W, Bizimis M, Morton P (2010) Determination of Mn, Fe, Co, Ni, Cu, Zn, Cd and Pb in seawater using high resolution magnetic sector inductively coupled mass spectrometry (HR-ICP-MS). *Anal Chim Acta* 665(2):200–207.
61. Martin JH, Knauer GA, Karl DM, Broenkow WW (1987) VERTEX: Carbon cycling in the northeast Pacific. *Deep Sea Res A, Oceanogr Res Pap* 34(2):267–285.